

Pump-Controlled Directional Light Emission from Random Lasers

Thomas Hisch,^{1,*} Matthias Liertzer,¹ Dionyz Pogany,² Florian Mintert,³ and Stefan Rotter^{1,†}

¹*Institute for Theoretical Physics, Vienna University of Technology,
Wiedner Hauptstraße 8–10/136, 1040 Vienna, Austria, EU*

²*Institute for Solid State Electronics, Vienna University of Technology, Floragasse 7, 1040 Vienna, Austria, EU*

³*Freiburg Institute for Advanced Studies, Albert–Ludwigs University of Freiburg, Albertstraße 19, 79104 Freiburg, Germany, EU*
(Dated: November 10, 2018)

The angular emission pattern of a random laser is typically very irregular and difficult to tune. Here we show by detailed numerical calculations that one can overcome the lack of control over this emission pattern by actively shaping the spatial pump distribution. We demonstrate, in particular, how to obtain customized pump profiles to achieve highly directional emission. Going beyond the regime of strongly scattering media where localized modes with a given directionality can simply be selected by the pump, we present an optimization-based approach which shapes extended lasing modes in the weakly scattering regime according to any predetermined emission pattern.

PACS numbers: 42.55.Zz, 42.25.Fx

The scattering of waves in a disordered medium is a ubiquitous physical process that occurs in a variety of different scenarios ranging from the micro- to the macroscale [1, 2]. Although much attention has been devoted to this topic, new intriguing phenomena continue to emerge in this area of physics [3]. Particularly exciting progress has recently been reported from the field of disordered photonics [4]: randomly scattering materials with optical gain were shown to operate as lasers despite the absence of a cavity [5]. In contrast to conventional lasers, however, such *random lasers* emit light at multiple frequencies and with a broad spatial emission profile [5–7]. On the other hand, unprecedented control of light fields in complex media has been achieved through optical *wave front shaping* based on spatial light modulators [8]. This progress has, e.g., enabled the spatial and temporal focusing of light or the projection and retrieval of images through strongly scattering media [9–13].

In the present Letter we strive to bridge the advances in the above two fields in order to tackle the longstanding goal [14–18] of making random lasers externally tunable. Employing a quasi-one-dimensional (1D) laser, it was recently shown numerically [16] as well as experimentally [17] that, using wave front shaping techniques to iteratively optimize the pump profile applied to a random laser, a single-mode lasing operation can be achieved at a predetermined frequency. With this approach one of the major deficiencies of a random laser, i.e., the lack of control over its emission frequency could be remedied. This leaves random lasers with the major drawback of emitting into arbitrary directions – a property which severely limits their applicability in many practical circumstances. Ideally, of course, the control over the angular emission pattern could also be exerted through the applied pump profile which is the most easily tunable control knob in a random laser. Demonstrating this explicitly seems, however, a formidable theoretical challenge. Consider, for comparison, the complexity involved

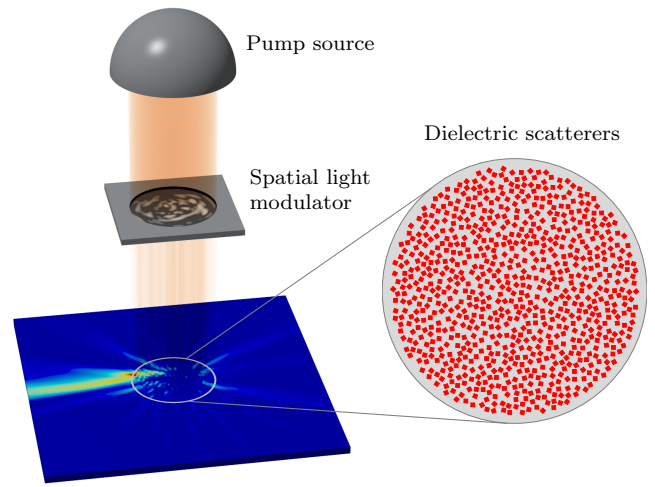


FIG. 1. (Color online) Sketch of the envisioned setup for realizing pump-controlled emission from a random laser: Before being directed to the random medium, an applied pump beam is sent through a spatial light modulator (SLM) which shapes the beam following an optimization procedure. The targeted emission pattern can be chosen at will. The geometry of the disk-shaped random laser (radius $R = 1 \mu\text{m}$) consists of square shaped scatterers with index n_s (red), embedded in a uniform background medium with index $n_b = 1$ (gray).

in previous demonstrations of pump optimization for random lasers [15–18] or in the well-studied problem of engineering a microcavity laser with unidirectional emission [19]. In both of these two cases, the functions which were optimized in one or several sequential steps were strictly one-dimensional: For the random lasers this function is related to the spatial pump profile and for the microcavity lasers it is the cavity boundary. In contrast, for fully controlling the emission pattern of a random laser one has to deal with an essentially two-dimensional pump profile with a very large number of adjustable degrees of freedom.

We address this challenge numerically, employing standard semiclassical laser theory at lasing threshold [20]. Our dielectric random laser medium consists of a passive and active component, $\varepsilon = \varepsilon_c + \chi_g$, with the passive dielectric function ε_c given by a static and randomly generated as well as immobile distribution of square-shaped sub-wavelength scatterers (see Fig. 1). These scatterers, which all have the same index of refraction n_s , are suspended in a disk-shaped background material of index $n_b = 1$. Both the scatterers and the background medium are assumed to be optically active, with a quantum susceptibility χ_g that depends on the wave number k [21],

$$\chi_g = D_0 F(\mathbf{x}) \gamma(k), \quad \text{with } \gamma(k) = \frac{\gamma_\perp}{k - k_a + i\gamma_\perp}. \quad (1)$$

This active component is subject to a position-dependent external pump source $F(\mathbf{x})$ as realized, e.g., with an optical pump beam controlled by a spatial light modulator (see schematic setup shown in Fig. 1). Here, D_0 defines an overall pump strength, k_a is the frequency of the atomic transition (we consider the speed of light $c = 1$) and $2\gamma_\perp$ is the width of the Lorentzian-shaped gain curve $|\gamma(k)|^2$. Note, that this approach is identical to the non-interacting form of the recently developed steady-state *ab initio* laser theory (SALT) [7, 22, 23], which provides the stationary solutions of the semiclassical Maxwell-Bloch equations. We can therefore make use of several parts of the efficient methods developed for SALT in the optimization problem at hand. In particular, we will employ the so-called threshold constant flux (TCF) states u_n defined by the non-Hermitian eigenvalue problem [23],

$$\{\nabla^2 + k^2 [\varepsilon_c(\mathbf{x}) + \eta_n(k) F(\mathbf{x})]\} u_n(\mathbf{x}, k) = 0. \quad (2)$$

These states $u_n(\mathbf{x}, k)$ and the corresponding eigenvalues $\eta_n(k)$, which we parametrize over the wave number k outside of the disk, are self-orthogonal with respect to the pump profile $F(\mathbf{x})$. They furthermore have the important property that each *threshold laser mode* (TLM) $\bar{\Psi}_i$, which we are interested in, is identical to one of these states, $u_{\bar{n}}(\mathbf{x})$. (Note that, throughout the Letter, we will use overbars to denote quantities at the lasing threshold.) The corresponding required pump strength \bar{D}_0^i and frequency \bar{k}_i at threshold are obtained from the threshold condition $\eta_{\bar{n}}(\bar{k}_i) = \gamma(\bar{k}_i) \bar{D}_0^i$ [23, 24]. We solve (2) using a high-order finite element method which efficiently copes with the finite-sized scatterers and the spatially varying pump profile $F(\mathbf{x})$ [25].

The task that we address within the above framework is to shape the emission pattern of the TLM which has the lowest (first) pump threshold \bar{D}_0^1 . Considering the scatterers of our disk-shaped random medium $\varepsilon_c(\mathbf{x})$ as well as the gain curve $\gamma(k)$ to be immobile (as in most experiments), we only tune the applied pump profile $F(\mathbf{x})$ such that the laser emission at threshold becomes unidirectional. To quantify the unidirectionality of a laser mode

we evaluate its far-field profile $\text{FFP}(\varphi)$ for a certain pump configuration, which is characterized by a set of complex expansion coefficients $\{\beta_{m,n}\}$ in a Bessel-function basis that respects the circular symmetry of the disk boundary [26]. Next, we introduce a weight \mathcal{D} which measures the overlap of the far-field profile $\text{FFP}(\varphi)$ of this mode with a desired profile $G(\varphi)$,

$$\mathcal{D}(\bar{\Psi}_1) = \frac{\int_0^{2\pi} G(\varphi) \text{FFP}[\varphi; \bar{\Psi}_1(\mathbf{x})] d\varphi}{\sqrt{\int_0^{2\pi} G^2 d\varphi \int_0^{2\pi} \text{FFP}^2 d\varphi}}, \quad (3)$$

where the denominator ensures that the weight is normalized such that $\mathcal{D} \in [0, 1]$. Choosing for the target function $G(\varphi)$ a narrow Gaussian profile centered around $\varphi = 180^\circ$ [see peak in Fig. 2(c)], we can formulate the goal of unidirectional emission in this direction as an optimization problem for the coefficients $\{\beta_{m,n}\}$ to be tuned such that $\mathcal{D} \rightarrow 1$.

Before going into the details of the optimization procedure, let us first generally assess the applicability of our approach for a dielectric featuring the two competing terms, $\varepsilon = \varepsilon_c + \chi_g$, of the passive and the active medium, respectively. Depending on which one of the two terms dominates, the structure of the lasing modes will be determined either by the passive medium or by the pump function. Correspondingly, our approach based on controlling the pump profile will have to be customized for each of these two limits.

In the regime of *strong* disorder, where ε_c dominates over χ_g , the disorder itself will strongly trap modes with, correspondingly, a high Q factor and a low lasing threshold. The structure of these lasing modes is thus mostly determined by the distribution of scatterers and not by the pump profile. Rather than *optimizing* the latter, we can here just choose a pump profile that simply *selects* the mode with the smallest deviation from the desired unidirectional far-field pattern to be the first lasing mode [18, 27, 28].

The situation is very different in the opposite limit of *weak* disorder, where χ_g dominates over ε_c . As no high-Q modes exist from the outset, also mode selection does not work. Rather, the pump profile has to be optimized such as to *shape* the modes in a way to be explored below. Since the case of strong disorder yields directional emission in a straightforward way, it provides a natural benchmark to gauge the quality of the emission patterns obtained for weakly disordered samples. We will thus describe both the weak and the strong disorder case, which we realize by a different contrast between the refractive index of the rectangular scatterers n_s in our sample and the background index, $n_b = 1$.

Let us first examine the limit of strong disorder, for which we choose $n_s = 3$. In this limit, the TCF states $u_n(\mathbf{x}, k)$ resulting from Eq. (2) with uniform pumping, $F(\mathbf{x}) = \text{const.}$, are strongly localized in space [28]. Among these high-Q modes we also find many modes

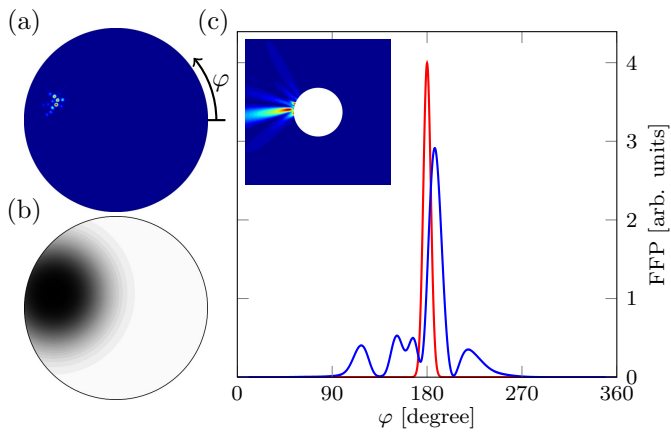


FIG. 2. (color online) First threshold laser mode $\bar{\Psi}_1$ at $k_1 = 29.82 \mu\text{m}^{-1}$ of a random laser in the strongly scattering regime (see Fig. 1 with $n_s = 3.0$). Shown are (a) the mode profile $|\bar{\Psi}_1(\mathbf{x})|$ inside the random laser, (b) the Gaussian-shaped pump profile that selects the mode (darker means more pump) and (c) the far-field profile (wiggly curve, blue) as well as the desired emission profile used as a reference (narrow peak, red). The inset in (c) depicts the near field directly outside the random laser disk and is complementary to (a). Note that the best directionality of a localized mode ($\mathcal{D} = 48.19\%$) matches the desired profile only approximately. The employed gain curve has a center frequency at $k_a = 30.0 \mu\text{m}^{-1}$ and a width of $\gamma_\perp = 0.2 \mu\text{m}^{-1}$. For better visibility the linear color functions used in the plots differ in absolute scale.

near the boundary of the disorder region with, correspondingly, a very narrow emission profile. To achieve the goal of directional emission, e.g., in the direction of $\varphi = 180^\circ$, we just need to focus the pump beam on the mode that emits most pronouncedly in this direction to make it lase first [28]. We demonstrate this explicitly with the example shown in Fig. 2, where a directional lasing mode is considered, which is the second TLM for the uniformly pumped device. Focusing a Gaussian shaped pump beam on the center of the region where this mode is localized, we can rearrange the modes such that this desired mode has the lowest lasing threshold of all. We have explicitly tested this pump selection procedure for a number of modes with different orientation of directional emission and found it to work very well, provided that enough directional modes are available and the gain curve is broad enough to be able to select them.

In the weak disorder limit, for which we choose $n_s = 1.2$, the lasing modes are extended, overlapping and their shape strongly depends on the pump profile $F(\mathbf{x})$ [7]. Simple mode selection is thus ruled out and a more sophisticated optimization is required instead. We start with an adjustable pump profile characterized by 153 complex expansion coefficients $\{\beta_{m,n}\}$ [26]. An optimization procedure is now employed to determine these parameters such that the far-field emission profile $\text{FFP}(\varphi)$

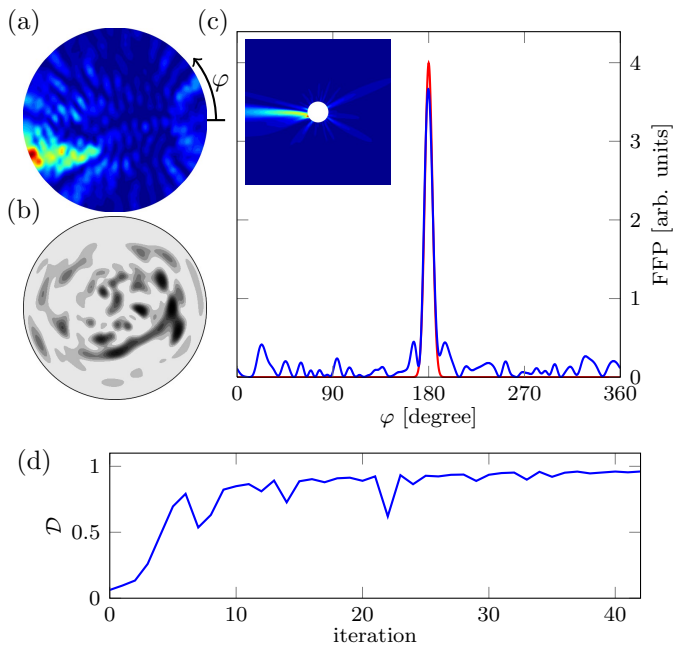


FIG. 3. (Color online) First threshold laser mode $\bar{\Psi}_1$ at $k_1 = 30.00 \mu\text{m}^{-1}$ of a random laser in the *weakly* scattering regime (see Fig. 1 with $n_s = 1.2$). Shown are (a) the optimized mode profile $|\bar{\Psi}_1(\mathbf{x})|$ inside the random laser, (b) the corresponding pump profile resulting from the optimization algorithm and (c) the far-field profile featuring a directionality of $\mathcal{D} = 96.08\%$. The inset in (c) shows the near field of the laser mode, just outside the pumped disk. Note the very good agreement which we find in the main panel of (c) between the optimized emission pattern (wiggly curve, blue) and the targeted Gaussian emission profile $G(\varphi)$ (narrow peak, red) centered at $\varphi = 180^\circ$ and with a width of 8.3° . In (d) the directionality is shown with respect to the number of iterations used in the optimization procedure. The parameters of the employed gain curve are $k_a = 30.0 \mu\text{m}^{-1}$ and $\gamma_\perp = 0.01 \mu\text{m}^{-1}$.

follows the desired narrow shape $G(\varphi)$ or, equivalently, $\mathcal{D} \rightarrow 1$ in Eq. (3). Note that our algorithm always optimizes the first TLM (which is determined for each iteration step anew) such that our laser stays single mode during the optimization procedure. Note also that it is clearly unfeasible to find the *unique* global maximum for $\mathcal{D}(\bar{\Psi}_1)$ in the extremely large parameter space of the above complex coefficients. Instead, we start with random initial guesses for the pump profile coefficients $\{\beta_{m,n}\}$ which we further refine locally by a gradient-based optimization [29]. For the local optimization procedure one needs to evaluate the gradient of the directionality $\nabla \mathcal{D}$ with respect to the expansion coefficients $\{\beta_{m,n}\}$. Because of the large number of involved parameters, it is crucial to devise a very fast and sufficiently accurate scheme to evaluate the gradient, which task can be solved with the help of the TCF state basis and its self-orthogonality property [26].

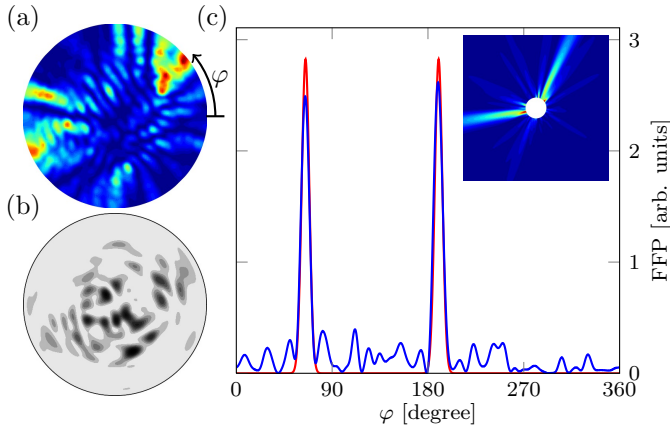


FIG. 4. (Color online) Results from the optimization of the random laser for emitting into two prescribed directions (65° and 190°) simultaneously (the same disorder is used as in Fig. 3). Shown are (a) the optimized mode profile $|\Psi_1(\mathbf{x})|$ inside the random laser, (b) the corresponding pump profile resulting from the optimization algorithm and (c) the far-field profile featuring a convergence degree of $\mathcal{D} = 96.12\%$. The inset in (c) shows the near field of the laser mode, just outside the pumped disk. Note the very good agreement which we find in the main panel of (c) between the optimized emission pattern (wiggly curve, blue) and the targeted double-peak emission profile $G(\varphi)$ (narrow peaks, red).

In Fig. 3(d) we display the progression of the directionality \mathcal{D} of the first TLM during the optimization procedure which leads to a rather quick convergence (in 42 iterative steps) from an initially random starting point to a nearly optimal mode with the desired directionality. The directionality does not increase monotonically as both the gradient of the directionality is only approximate and the first TLM can switch between modes [26]. Note also that typically several random starting conditions for the iteration are necessary due to the existence of local maxima of $\mathcal{D}(\{\beta_{m,n}\})$ in the multidimensional parameter space of $\{\beta_{m,n}\}$ where the local optimization may get stuck. More sophisticated methods to overcome local maxima could certainly be applied here. Since, however, we already do reach excellent results with $\mathcal{D} > 96\%$ with typically not more than altogether 20 initial guesses, such methods are not compulsory. The mode which matches the emission pattern of the target function $G(\varphi)$ best and the corresponding pump profile are shown in Fig. 3. This encouraging result is directly reflected by the shape of the corresponding lasing mode shown in Fig. 3(a) and 3(c) which displays the desired narrow, beamlike shape outside of the disk boundary. We emphasize, in particular, that the directionality can here be much better controlled than in strongly disordered media. This is best observed by comparing Figs. 2 and 3: Although the mode which agrees best with the desired emission profile $G(\varphi)$ is selected in the strongly scattering medium (Fig. 2), a clear

deviation from the desired target function $G(\varphi)$ can be observed. In fact, for disorder configurations different than the one in Fig. 2 we observed much larger deviations. For weakly scattering media, on the contrary, the applied pump profile is optimized for each specific distribution of scatterers such that a directionality of $\mathcal{D} \gtrsim 95\%$ is generally guaranteed.

Our optimization procedure can be pushed even further in the sense that the reference emission pattern $G(\varphi)$ is not limited to a function with a single narrow peak, but instead can be chosen almost arbitrarily. As an example we have also optimized the pump profile such that the random laser emits into two directions simultaneously; see Fig. 4. This result shows the versatility of our approach and manifests that the emission of a weakly scattering random laser can be arbitrarily shaped using a carefully optimized pump profile. Combining this technique together with the frequency selection mechanism presented in [16, 17] suggests that random lasers can be controlled on an unprecedented scale.

We emphasize that the pump profiles which give rise to these uni- or multidirectional lasing states are neither very focused (as in [18, 28]), nor strip-shaped (as in [30, 31]), nor in any other way evidently self-explanatory. Instead, the obtained profiles are structured on a scale comparable to the lasing wavelength – a situation that is routinely created in laboratory experiments [9–12, 17]. The pump optimization procedure presented above can, in principle, be mapped to a corresponding experiment using, e.g., a spatial light modulator for shaping the pump beam (see Fig. 1). In this case the optimization can be organized through a feedback loop between the measured emission and the applied pump profile, as implemented very recently in a similar setting [17]. Realizing such ideas in the experiment would not only be interesting for fundamental research on light profile patterning in a disordered medium, but would constitute a major step forward in bringing random lasers closer to practical applications where specific emission profiles are required.

The authors would like to thank N. Bachelard, S. Gigan and P. Sebbah for carefully reading our manuscript and the following colleagues for very fruitful discussions: S. Esterhazy, D. Krimer, J. M. Melenk, and J. Schöberl. Financial support by the Vienna Science and Technology Fund (WWTF) through Project No. MA09-030, by the European Research Council (ERC) (project ODYQUENT) and by the Austrian Science Fund (FWF) through Projects No. F25-14 (SFB IR-ON), No. F49-P10 (SFB NextLite) is gratefully acknowledged. We are also indebted to the administration of the Vienna Scientific Cluster (VSC) for generously granting us access to computational resources.

-
- * t.hisch@gmail.com
† stefan.rotter@tuwien.ac.at
- [1] E. Akkermans and G. Montambaux, *Mesoscopic Physics of Electrons and Photons* (Cambridge University Press, 2007).
 - [2] V. Letokhov and S. Johansson, *Astrophysical Lasers* (Oxford University Press, 2008).
 - [3] P. Barthelemy, J. Bertolotti, and D. S. Wiersma, *Nature* **453**, 495 (2008); L. Sapienza, H. Thyrestrup, S. Stobbe, P. D. Garcia, S. Smolka, and P. Lodahl, *Science* **327**, 1352 (2010); J. Wang and A. Z. Genack, *Nature* **471**, 345 (2011); Q. Baudouin, N. Mercadier, V. Guarnera, W. Guerin, and R. Kaiser, *Nat. Phys.* **9**, 357 (2013).
 - [4] D. S. Wiersma, *Nat. Photon.* **7**, 188 (2013).
 - [5] H. Cao, *Waves in Random Media* **13**, R1 (2003); D. S. Wiersma, *Nat. Phys.* **4**, 359 (2008); O. Zaitsev and L. Deych, *Journal of Optics* **12**, 024001 (2010).
 - [6] H. Cao, Y. Ling, J. Y. Xu, A. L. Burin, and R. P. H. Chang, *Physica B: Condensed Matter* **338**, 215 (2003).
 - [7] H. E. Türeci, L. Ge, S. Rotter, and A. D. Stone, *Science* **320**, 643 (2008); H. E. Türeci, A. D. Stone, L. Ge, S. Rotter, and R. J. Tandy, *Nonlinearity* **22**, C1 (2009).
 - [8] A. P. Mosk, A. Lagendijk, G. Lerosey, and M. Fink, *Nat. Photon.* **6**, 283 (2012).
 - [9] I. M. Vellekoop and A. P. Mosk, *Opt. Lett.* **32**, 2309 (2007).
 - [10] S. Popoff, G. Lerosey, M. Fink, A. C. Boccara, and S. Gigan, *Nat. Commun.* **1**, 81 (2010); S. M. Popoff, G. Lerosey, R. Carminati, M. Fink, A. C. Boccara, and S. Gigan, *Phys. Rev. Lett.* **104**, 100601 (2010).
 - [11] O. Katz, E. Small, Y. Bromberg, and Y. Silberberg, *Nat. Photon.* **5**, 372 (2011).
 - [12] J. Aulbach, B. Gjonaj, P. M. Johnson, A. P. Mosk, and A. Lagendijk, *Phys. Rev. Lett.* **106**, 103901 (2011).
 - [13] S. Rotter, P. Ambichl, and F. Libisch, *Phys. Rev. Lett.* **106**, 120602 (2011).
 - [14] D. S. Wiersma and S. Cavaleri, *Nature* **414**, 708 (2001); K. Lee and N. M. Lawandy, *Optics Communications* **203**, 169 (2002); X. H. Wu, A. Yamilov, H. Noh, H. Cao, E. W. Seelig, and R. P. H. Chang, *Journal of the Optical Society of America B* **21**, 159 (2004); S. Gottardo, S. Cavaleri, O. Yaroshchuk, and D. S. Wiersma, *Phys. Rev. Lett.* **93**, 263901 (2004); C. Vanneste and P. Sebbah, *Phys. Rev. E* **71**, 026612 (2005); T. Savels, A. P. Mosk, and A. Lagendijk, *Phys. Rev. Lett.* **98**, 103601 (2007); S. Gottardo, R. Sapienza, P. D. García, A. Blanco, D. S. Wiersma, and C. López, *Nat. Photon.* **2**, 429 (2008); H. Fujiwara, Y. Hamabata, and K. Sasaki, *Opt. Express* **17**, 3970 (2009); H. K. Liang, S. F. Yu, and H. Y. Yang, *Appl. Phys. Lett.* **97**, 241107 (2010); R. Bardoux, A. Kaneta, M. Funato, K. Okamoto, Y. Kawakami, A. Kikuchi, and K. Kishino, *Opt. Express* **19**, 9262 (2011); R. G. S. El-Dardiry and A. Lagendijk, *Appl. Phys. Lett.* **98**, 161106 (2011); R. Frank, *Transport theory: Spatial coherence of random laser emission*, arXiv e-print 1209.4552 (2012); P. Stano and P. Jacquod, *Nat. Photon.* **7**, 66 (2013).
 - [15] M. Leonetti, C. Conti, and C. Lopez, *Nat. Photon.* **5**, 615 (2011).
 - [16] N. Bachelard, J. Andreasen, S. Gigan, and P. Sebbah, *Phys. Rev. Lett.* **109**, 033903 (2012).
 - [17] N. Bachelard, S. Gigan, X. Noblin, and P. Sebbah, *arXiv:1303.1398* (2013).
 - [18] M. Leonetti and C. López, *Appl. Phys. Lett.* **102**, 071105 (2013).
 - [19] C. Gmachl, F. Capasso, E. E. Narimanov, J. U. Nöckel, A. D. Stone, J. Faist, D. L. Sivco, and A. Y. Cho, *Science* **280**, 1556 (1998); J. Wiersig and M. Hentschel, *Phys. Rev. Lett.* **100**, 033901 (2008); C. H. Yi, M. W. Kim, and C. M. Kim, *Appl. Phys. Lett.* **95**, 141107 (2009); C. Yan, Q. J. Wang, L. Diehl, M. Hentschel, J. Wiersig, N. Yu, C. Pflügl, F. Capasso, M. A. Belkin, T. Edamura, M. Yamanishi, and H. Kan, *Appl. Phys. Lett.* **94**, 251101 (2009); Q. H. Song, L. Ge, A. D. Stone, H. Cao, J. Wiersig, J. B. Shim, J. Unterhinninghofen, W. Fang, and G. S. Solomon, *Phys. Rev. Lett.* **105**, 103902 (2010); Q. J. Wang, C. Yan, N. Yu, J. Unterhinninghofen, J. Wiersig, C. Pflügl, L. Diehl, T. Edamura, M. Yamanishi, H. Kan, and F. Capasso, *Proc. Natl. Acad. Sci. USA* **107**, 22407 (2010); S. Shinohara, T. Harayama, T. Fukushima, M. Hentschel, T. Sasaki, and E. E. Narimanov, *Phys. Rev. Lett.* **104**, 163902 (2010).
 - [20] H. Haken, *Light: Laser light dynamics* (North-Holland Pub. Co., 1985).
 - [21] A. E. Siegman, *Lasers* (University Science Books, 1986).
 - [22] H. E. Türeci, A. D. Stone, and L. Ge, *Phys. Rev. A* **76**, 013813 (2007).
 - [23] L. Ge, Y. D. Chong, and A. D. Stone, *Phys. Rev. A* **82**, 063824 (2010).
 - [24] M. Liertzer, L. Ge, A. Cerjan, A. D. Stone, H. E. Türeci, and S. Rotter, *Phys. Rev. Lett.* **108**, 173901 (2012).
 - [25] We employ the open source finite element mesher *netgen* (J. Schöberl, *Computing and Visualization in Science* **1**, 41 (1997)) and the corresponding solver NGSolve available from <http://sf.net/projects/ngsolve>
 - [26] See Supplemental Material at [] for the definition of the employed pump basis, the frequency variation of the first TLM in the course of the optimization procedure and for an efficient evaluation of the directionality gradient ∇D .
 - [27] J. Andreasen, C. Vanneste, L. Ge, and H. Cao, *Proceedings of SPIE* **7597**, 759713 (2010).
 - [28] C. Vanneste and P. Sebbah, *Phys. Rev. Lett.* **87**, 183903 (2001).
 - [29] We employ the *nlopt* toolkit using the Multi-Level Single-Linkage algorithm as the global optimization routine where a low-discrepancy sequence is used for the generation of random initial guesses. The method of moving asymptotes is used for the gradient-based local optimization. S. G. Johnson, "The NLOpt nonlinear-optimization package," (2012); K. Svanberg, *SIAM Journal on Optimization* **12**, 555 (2002); A. H. G. R. Kan and G. T. Timmer, *Mathematical Programming* **39**, 27 (1987); *Mathematical Programming* **39**, 57 (1987); S. Kucherenko and Y. Sytsko, *Computational Optimization and Applications* **30**, 297 (2005).
 - [30] X. Wu, W. Fang, A. Yamilov, A. A. Chabanov, A. A. Asatryan, L. C. Botten, and H. Cao, *Phys. Rev. A* **74**, 053812 (2006).
 - [31] L. Ge, *Steady-state Ab Initio Laser Theory and its Applications in Random and Complex Media*, PhD, Yale University (2010).

Supplemental material for pump-controlled directional light emission from random lasers

Thomas Hisch,^{1,*} Matthias Liertzer,¹ Dionyz
Pogany,² Florian Mintert,³ and Stefan Rotter^{1,†}

¹*Institute for Theoretical Physics, Vienna University of Technology,
Wiedner Hauptstraße 8–10/136, 1040 Vienna, Austria, EU*

²*Institute for Solid State Electronics, Vienna University of Technology,
Floragasse 7, 1040 Vienna, Austria, EU*

³*Freiburg Institute for Advanced Studies,
Albert–Ludwigs University of Freiburg,
Albertstraße 19, 79104 Freiburg, Germany, EU*

(Dated: November 10, 2018)

PUMP PROFILE BASIS

To first specify and then optimize the pump profile for directional emission we expand the two-dimensional pump profile $F(\mathbf{x})$ on the disk-shaped random laser of radius R using a Bessel function basis of the form $J_m(j_{m,n}|\mathbf{x}|/R)\exp[-im\varphi]$. Here the $j_{m,n}$ are the Bessel function roots, φ the polar angle, and R the radius of the disk within which the scatterers are randomly distributed. This basis has the suitable property of vanishing at the disk boundary outside of which no pump is applied. Inside the disk we expand the real and strictly positive pump function $F(\mathbf{x})$ as follows,

$$F(\mathbf{x}; \beta_{m,n}) = \left| \sum_{m,n} \beta_{m,n} J_m(j_{m,n} \frac{|\mathbf{x}|}{R}) \exp[-im\varphi] \right|^2, \quad (1)$$

where $\beta_{m,n}$ are complex expansion coefficients. In our numerical calculations we restrict the summation in Eq. (1) to the limits $m \in [-m_{\max}, m_{\max}]$ and $n \in [0, n_{\max}]$, corresponding to a finite resolution of the pump beam in radial and azimuthal direction, respectively. The choice which we make for the $(2m_{\max}+1) \times (n_{\max}+1)$ complex coefficients $\beta_{m,n}$ will determine the threshold laser mode $\bar{\Psi}_1(\mathbf{x})$. In the calculations presented in the main part of the article (see Fig. 3), we choose $n_{\max} = 8$ and $m_{\max} = 8$. Note that, although not explicitly shown here, one can reduce the complex parameters $\beta_{m,n}$ to purely real ones since only the absolute square of the superposition of states is considered.

EMISSION FREQUENCY BEHAVIOR

In the course of optimizing the directionality of the first TLM the changes in the pump profile also lead to slight variations of the laser frequency around the peak gain frequency of

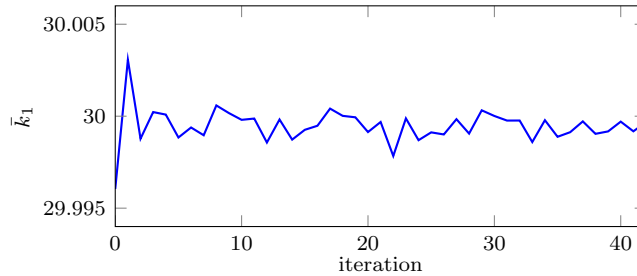


FIG. S1. Variation of the emission frequency \bar{k}_1 of the first threshold laser mode in the course of the optimization procedure (the same parameters were used here as for Fig. 3d in the main text).

$30 \mu m^{-1}$. For the specific case displayed in Fig. 3d of the main text this frequency variation takes on the form shown in Fig. S1. Note that for the first few iteration steps this variation is larger since the pump profile is modified more strongly here as compared to later steps of the optimization procedure.

DERIVATION OF THE GRADIENT OF THE DIRECTIONALITY

In order to efficiently calculate the gradient of the directionality \mathcal{D} with respect to the complex coefficients $\{\beta_{m,n}\}$ we approximate this gradient with the help of the TCF states which are defined as follows

$$\{\nabla^2 + \bar{k}_1^2 [\varepsilon_c(\mathbf{x}) + \eta_n(\bar{k}_1)F(\mathbf{x}, \bar{k}_1)]\} u_n(\mathbf{x}) = 0, \quad (2)$$

and which satisfy the self-orthogonality relation

$$\int_{r < R} u_i(\mathbf{x}) F(\mathbf{x}) u_j(\mathbf{x}) d\mathbf{x} = \delta_{i,j}. \quad (3)$$

The basis itself is calculated at the frequency \bar{k}_1 of the first threshold laser mode $\bar{\Psi}_1$, for which we optimize the angular emission pattern to match the targeted emission pattern $G(\varphi)$. In order to reduce the terminology in the following we rewrite, without loss of generality, the set of complex coefficients $\{\beta_{m,n}\}$ as a set of twice as many real coefficients α_i , where the imaginary part of the coefficients $\{\beta_{m,n}\}$ is moved into the corresponding basis function $f_i(\mathbf{x})$, such that,

$$F(\mathbf{x}; \beta_{m,n}) = \left| \sum_{m,n} \beta_{m,n} J_m(j_{m,n} \frac{|\mathbf{x}|}{R}) \exp[-im\varphi] \right|^2 \quad (4)$$

$$=: \left| \sum_i \alpha_i f_i(\mathbf{x}) \right|^2. \quad (5)$$

We will now derive the gradient of the directionality \mathcal{D} with respect to these coefficients α_i . The first part of this derivation follows directly from differentiation of \mathcal{D} with respect to

α_j ,

$$\frac{\partial}{\partial \alpha_j} \mathcal{D}[\{\alpha_i\}] = \partial_{\alpha_j} \int \tilde{G}(\varphi) \frac{\text{FFP}(\{\alpha_i\}, \varphi)}{\sqrt{\int \text{FFP}^2(\{\alpha_i\}, \varphi') d\varphi'}} d\varphi \quad (6)$$

$$= \int \tilde{G}(\varphi) \left[\frac{\partial_{\alpha_j} \text{FFP}(\{\alpha_i\}, \varphi)}{\sqrt{\int \text{FFP}^2(\{\alpha_i\}, \varphi') d\varphi'}} - \right. \quad (7)$$

$$\left. - \frac{\text{FFP}(\{\alpha_i\}, \varphi) \int \text{FFP}(\{\alpha_i\}, \varphi') \partial_{\alpha_j} \text{FFP}(\{\alpha_i\}, \varphi') d\varphi'}{(\int \text{FFP}^2(\{\alpha_i\}, \varphi') d\varphi')^{\frac{3}{2}}} \right] d\varphi, \quad (8)$$

where $\tilde{G}(\varphi) = G(\varphi)/\sqrt{\int G(\varphi')^2 d\varphi'}$ is the normalized reference emission profile and FFP is the angular far-field emission profile of the first TLM. The latter is determined as the real part of the complex Poynting vector at $r \rightarrow \infty$ which can be simplified to

$$\text{FFP}(\varphi) := \lim_{r \rightarrow \infty} \frac{r}{2\bar{k}_1} \text{Im}[\bar{\Psi}_1^*(r, \varphi) \partial_r \bar{\Psi}_1(r, \varphi)]. \quad (9)$$

The partial derivative of FFP with respect to the coefficients α_j is given by

$$\partial_{\alpha_j} \text{FFP}(\{\alpha_i\}, \varphi) = \lim_{r \rightarrow \infty} \frac{r}{2\bar{k}_1} \text{Im}[(\partial_{\alpha_j} \bar{\Psi}_1^*) \partial_r \bar{\Psi}_1 + \bar{\Psi}_1^* \partial_r (\partial_{\alpha_j} \bar{\Psi}_1)]. \quad (10)$$

For reasons of improved efficiency we express the gradient of the TLM $\partial_{\alpha_j} \bar{\Psi}_1$ in terms of the TCF states u_n . Note, that the first TLM $\bar{\Psi}_1$ is equivalent to a TCF state $u_{\bar{n}}$ evaluated at the threshold laser frequency \bar{k}_1 , i.e., $\bar{\Psi}_1(\mathbf{x}) = u_{\bar{n}}(\mathbf{x}, \bar{k}_1)$. With the help of this equivalence the gradient of $\bar{\Psi}_1$ is formally defined as

$$\partial_{\alpha_j} u_{\bar{n}} = \lim_{h \rightarrow 0} \frac{u_{\bar{n}}(\{\alpha_i + h\delta_{i,j}\}) - u_{\bar{n}}(\{\alpha_i\})}{h}. \quad (11)$$

We can now proceed and use perturbation theory in order to derive an expression for $\partial_{\alpha_j} u_{\bar{n}}$ explicitly. With the operator $\hat{L} = -\nabla^2 - \bar{k}_1^2 \varepsilon_c$ we can rewrite the original eigenvalue problem Eq. (2) as

$$\hat{L} u_n = \eta_n \bar{k}_1^2 F(\{\alpha_i\}) u_n \quad (12)$$

and the ‘‘perturbed’’ eigenvalue problem as

$$\hat{L} \tilde{u}_n = \tilde{\eta}_n \bar{k}_1^2 F(\{\alpha_i + h\delta_{i,j}\}) \tilde{u}_n, \quad (13)$$

where the perturbed state $\tilde{u}_n = u_n(\{\alpha_i + h\delta_{i,j}\})$ and the perturbed eigenvalue $\tilde{\eta}_n = \eta_n(\{\alpha_i +$

$h\delta_{i,j}\}$). The perturbed pump profile can be approximated by

$$F(\{\alpha_i + h\delta_{i,j}\}) = \left| \sum_i \alpha_i f_i(x) + h f_j(x) \right|^2 \quad (14)$$

$$= F(\{\alpha_i\}) + h \underbrace{\sum_i 2\alpha_i \text{Re}(f_i f_j^*)}_{F'(\{\alpha_i\})} + \mathcal{O}(h^2). \quad (15)$$

In a next step we insert this approximation, together with the following ansatz for the perturbed eigenstate,

$$\tilde{u}_{\bar{n}} \approx u_{\bar{n}} + h \sum_{\substack{i=1 \\ i \neq \bar{n}}}^N c_{i,\bar{n}} u_i, \quad (16)$$

and for the eigenvalue, $\tilde{\eta}_n = \eta_n + h\eta'_n$, into Eq. (13) (N denotes here the size of the TCF basis). By discarding terms of $\mathcal{O}(h^2)$ and making use of the self-orthogonality of the TCF-states [Eq. (3)] we obtain the expansion coefficients of the perturbed TCF state,

$$c_{i,\bar{n}} = \frac{\eta_{\bar{n}}}{\eta_i - \eta_{\bar{n}}} \int_{r < R} u_i(\mathbf{x}) F'(\{\alpha_i\}) u_{\bar{n}}(\mathbf{x}) d\mathbf{x}, \quad (17)$$

where R is the radius of our random laser disk. This expression can then be inserted back into Eq. (16), which yields

$$\partial_{\alpha_j} u_{\bar{n}} = \sum_{\substack{i=1 \\ i \neq \bar{n}}}^N c_{i,\bar{n}} u_i. \quad (18)$$

With this expression and Eq. (10), the desired approximate gradient of the directionality measure \mathcal{D} with respect to the coefficients α_i , Eq. (8), is now easily evaluated.